

Crystal field analysis and emission cross sections of Ho^{3+} in the locally disordered single-crystal laser hosts $M^+\text{Bi}(\text{XO}_4)_2$ ($M^+=\text{Li, Na}$; $X=\text{W, Mo}$)

A. Méndez-Blas,* M. Rico, V. Volkov, C. Zaldo, and C. Cascales†

Instituto de Ciencia de Materiales de Madrid, Consejo Superior de Investigaciones Científicas, Cantoblanco, 28049 Madrid, Spain

(Received 15 November 2006; revised manuscript received 16 April 2007; published 24 May 2007)

The spectroscopic properties of Ho^{3+} laser channels in locally disordered tetragonal $\text{NaBi}(\text{WO}_4)_2$ (NaBiW), $\text{NaBi}(\text{MoO}_4)_2$ (NaBiMo), and $\text{LiBi}(\text{MoO}_4)_2$ (LiBiMo) single crystals grown by the Czochralski method have been studied in the 5–300-K temperature range using several holmium concentrations $[\text{Ho}] \approx 0.05\text{--}0.6 \times 10^{20} \text{ cm}^{-3}$. Here 5-K polarized optical absorption and photoluminescence measurements have been used to determine the energy position of 85, 56, and 39 Ho^{3+} Stark levels in NaBiW , NaBiMo , and LiBiMo crystals, respectively. These energy levels were labeled with irreducible representations corresponding to the S_4 local symmetry of an average optical center. Single-electron Hamiltonians combining together free-ion and crystal-field interactions have been used in the fit of experimental energy levels and in the simulation of the corresponding $4f^{10} \text{Ho}^{3+}$ configuration for NaBiW and NaBiMo crystals. Very satisfactory correlations were obtained between experimental and calculated crystal-field levels, with rms deviations $\sigma=8.8$ and 7.3 cm^{-1} for NaBiW and NaBiMo , respectively. The radiative properties and emission cross sections of Ho^{3+} laser channels in these hosts were calculated by the Judd-Ofelt theory and compared with experimental results. The emission cross sections of Ho^{3+} in NaBiW are similar to those observed in other crystal laser hosts, and positive gain cross sections can be achieved in extended spectral ranges. These properties make the Ho^{3+} -doped double tungstates and double molybdates feasible materials for tunable and short-pulse laser operation.

DOI: 10.1103/PhysRevB.75.174208

PACS number(s): 61.43.-j, 78.20.-e, 78.55.-m, 42.55.Rz

I. INTRODUCTION

Disordered crystals with inhomogeneously broadened optical bands are presently being searched for in the context of ultrafast (femtosecond) laser systems.¹ Tetragonal double tungstate (DT) and double molybdate (DMo) single crystals with general formula $MT(\text{XO}_4)_2$ (M =monovalent, T =trivalent, and $X=\text{W}^{6+}$ or Mo^{6+} ions) are a class of locally disordered compounds related to the CaWO_4 scheelite type. For brevity we shall refer to each particular DT or DMo compound as MTX . The substitution of two Ca^{2+} ions by an M^+T^{3+} pair gives rise to a large number of compounds, some of them exhibiting polymorphism; therefore, different crystallographic structures (triclinic, monoclinic, orthorhombic, etc.) can be selected.² LiLaW ,³ LiTmO ($T=\text{Bi}$,⁴ Y ,⁵ La ,⁵ Ce-Lu ⁵), NaTW ($T=\text{Bi}$,⁴ Y ,⁶ La ,⁶ Nd-Er ⁶), NaTmO ($T=\text{Bi}$,⁴ Y ,⁷ La ,⁸ Gd ⁸), KLaMo ,⁹ and AgLaW ,¹⁰ compounds have congruent melt, and the tetragonal crystallographic phase is stable upon cooling from their congruent melting points to room temperature. Single crystals of these compounds can be grown in air by the Czochralski method, with high growth rates (typically 1 mm/h) and a relatively low crystal cost, which ease their applications.

The most common trivalent lanthanide Ln^{3+} ions of interest for laser operation are $\text{Ln}^{3+}=\text{Pr, Nd, Ho, Er, Tm, and Yb}$. The f electrons of Yb^{3+} and Tm^{3+} experience a stronger interaction with the vibrational lattice environment, and therefore these ions are well suited for tuning and mode-locked laser operation even in ordered crystals. The broad bandwidths are also useful for pumping with commercial (non-wavelength-matched) semiconductor diodes without thermal stabilization, leading to low-cost systems. Another outstanding application already demonstrated in some DT and DMo crystals is solid-state stimulated Raman laser shifting

(SRS).¹¹ Tetragonal DT and DMo crystals have larger Raman bandwidths [full width at half maximum (FWHM) $\approx 15 \text{ cm}^{-1}$] than the ordered phases of DT and DMo compounds, like monoclinic $\text{KY}(\text{WO}_4)_2$ (FWHM $\approx 5 \text{ cm}^{-1}$), leading thus to operation in shorter SRS picosecond regimes.¹² When the other Ln^{3+} (Pr-Er) are considered, the above applications require spectral inhomogeneous broadening. In tetragonal DT and DMo the spectral broadening derives from two features of the crystal host: the overlapping Ln^{3+} contributions arising from two shared crystal sites $2b$ and $2d$ and the broadening associated to structural disorder—that is, the optical centers resulting from different short-range M and T distributions around each one of the two above Ln^{3+} lattice sites.

Laser tunability and mode-locked operation have been recently achieved by using Yb^{3+} - and Tm^{3+} -doped tetragonal DT and DMo hosts: for Yb^{3+} a continuous tuning range up to 65 nm has been reached around $1.05 \mu\text{m}$,¹³ and 212 nm around $1.93 \mu\text{m}$ has been also realized with Tm^{3+} .¹⁴ The tuning ranges so far demonstrated were limited by the spectral responses of the optical cavity elements (mirrors and birefringent filter), and then even broader tuning ranges are expected. The estimated full tuning range can be used in mode-locked operation to produce <50 -fs laser pulses. First steps in this direction have already shown pulses of 120 fs in Yb -doped NaGdW ¹³ and 90 fs in Yb -doped NaLuW .¹⁵ To achieve similar results for other laser-active Ln^{3+} (Pr-Er) in DT and DMo still remains a challenging task. Knowledge of the spectroscopic ion properties is required to evaluate this possibility.

$\text{NaBi}(\text{WO}_4)_2$ (NaBiW), $\text{NaBi}(\text{MoO}_4)_2$ (NaBiMo), and $\text{LiBi}(\text{MoO}_4)_2$ (LiBiMo) single crystals have a locally disordered tetragonal crystallographic structure with space group (SG) $I\bar{4}$.¹⁶ Laser operation of Ln^{3+} in NaBiW , and NaBiMo

was first shown using Nd^{3+} .¹⁷ In the present work we study Ho^{3+} in NaBiW, NaBiMo, and LiBiMo as a potential laser ion for the visible and midinfrared regions.¹⁸ Although Ho^{3+} lacks a strong absorption for diode pumping at $\lambda = 800\text{--}1000$ nm, it can be sensitized in this region by Tm^{3+} and Yb^{3+} codoping¹⁹ or pumped directly with the $\lambda \approx 1.9$ μm emissions of GaInAsSb/AlGaAsSb quantum-well diodes and Tm lasers using a pumping cascade scheme. Therefore, Ho^{3+} remains of wide interest in present laser technology.²⁰

Using low-temperature (5 K) polarized spectroscopic techniques and crystal field modeling we have determined the Ho^{3+} Stark energy levels from 5I_8 up to 3H_6 (for NaBiW) or 5G_5 (for NaBiMo and LiBiMo) manifolds, which have been labeled with the adequate irreducible representation (IR) for the current S_4 local symmetry, and the large bandwidth of the spectral bands has been confirmed. Radiative and nonradiative processes of these Ho^{3+} materials have been studied in detail to evaluate the application as solid-state laser systems.

II. GROWTH PROCEDURES AND CRYSTAL STRUCTURE

The Czochralski crystal growth procedures of NaBiW, NaBiMo, and LiBiMo have been described previously.^{4,16} Ho-doped single crystals with optical quality were obtained reacting the host compounds with 99.9% Ho_2O_3 from CERAC Inc. during ~ 100 h at 1133 K for tungstates and 1058 K for molybdates. The products were melted in Pt crucibles, and crystals were pulled at the following rates: 0.8–4 mm/h for NaBiW, 1.3–2.3 mm/h for NaBiMo, and 1.7–1.9 mm/h for LiBiMo.

The Ho concentration in the crystal $[\text{Ho}]_{\text{cryst}}$ was determined by proton-induced x-ray emission (PIXE) spectroscopy using for each host samples of the highest Ho concentration available. For this purpose we used $L_{\alpha 1, \alpha 2}$ holmium x-ray emission at about 6.719 keV, which was free of interference with x-ray emissions from other crystal constituents. Samples were irradiated in vacuum with 2.0-MeV protons supplied by a 2.5-MV Van de Graaff accelerator. The proton beam was collimated down to 1.5 mm in diameter, and beam currents close to 3 nA were used. A 165-eV-resolution Si(Li) detector was placed at 110° relative to the proton beam direction, and the face of the sample was tilted to an angle of 15° with the incident beam. Spectra analyses were performed by the AXIL-PC V3.1 computer code. Quantitative analysis was carried out through the DATPIXE program, which accounts for proton energy loss.²¹

The Ho content for lower concentrations was determined by comparison of the optical absorption (OA) intensities. Table I summarizes the results obtained. It is worth noting that the segregation coefficient $S = [\text{Ho}]_{\text{cryst}}/[\text{Ho}]_{\text{melt}}$ of holmium in Bi-based DT and DMO is larger than 1, in agreement with previous results of other lanthanides.⁴

In the noncentrosymmetric tetragonal SG $\bar{I}4$ (No. 82), $Z=2$, Li^+/Na^+ and Bi^{3+} cations share two nonequivalent lattice sites $2d$ and $2b$, both with S_4 local symmetry and the same high-symmetry axis parallel to the crystal c axis, but with different occupancy factors: namely, 63(60)% Bi

TABLE I. Holmium concentration in NaBiW, NaBiMo, and LiBiMo crystals used in this work. The Ho concentration in low-doped samples was deduced from a comparison of the Ho^{3+} optical absorption (OA) taken as reference the PIXE results.

| | $[\text{Ho}]_{\text{melt}}$ [mol %] | $[\text{Ho}]_{\text{cryst}}$ [mol %] | $[\text{Ho}]_{\text{cryst}}$ [10^{20} cm^{-3}] |
|--------|--|---|---|
| NaBiW | 0.02 | 0.11 | 0.07 OA |
| | 0.31 | 0.56 | 0.35 PIXE |
| NaBiMo | 0.02 | 0.10 | 0.06 OA |
| | 0.10 | 0.48 | 0.30 OA |
| | 0.33 | 1.09 | 0.68 PIXE |
| LiBiMo | 0.02 | 0.08 | 0.05 OA |
| | 0.10 | 0.31 | 0.20 OA |
| | 0.32 | 0.64 | 0.41 PIXE |

+37(40)% Na and 46(40)% Bi+54(60)% Na for $2d$ and $2b$ sites, respectively, in NaBiW,^{16,22} 45% Bi+55% Na and 53% Bi+47% Na in NaBiMo,¹⁶ or 0.52% Bi+0.48% Li and 0.51% Bi+0.49% Na in LiBiMo, for $2d$ and $2b$ sites,¹⁶ respectively. In these crystals as well as in other isostructural DT and DMO, detailed crystallographic analyses have shown that Ln^{3+} active ions replace $\text{Bi}^{3+}(\text{T}^{3+})$ in both sites: Er^{3+} in NaBiW, NaBiMo, and LiBiMo,¹⁶ Yb^{3+} in NaGdW,¹³ and Yb^{3+} in LiGdMo.²³

III. EXPERIMENTAL TECHNIQUES

Ground-state optical absorption (GSA) was recorded in a Varian spectrophotometer model CARY-5E. Photoluminescence (PL) was excited with a cw Ar^+ laser or with Rhodamine R-6G ($\lambda \approx 591$ nm) and Coumarin-480 ($\lambda \approx 485$ nm) emissions of a dye laser (LSI, model DUO-220). The holmium emission was dispersed with a SPEX 340E spectrometer using 1200- or 600-1/mm gratings. The light was detected with a water-cooled R2658 Hamamatsu InGaAs photomultiplier ($\lambda = 0.0185\text{--}0.1030$ μm) and a 77-K-cooled Ge photodiode ($\lambda = 0.8\text{--}1.7$ μm). PL emissions were corrected by the spectral response of the equipment, which was previously determined using a calibrated W lamp standard. The intensity of the $^5F_5 \rightarrow ^5I_7$ and $^5S_2 \rightarrow ^5I_6$ transitions has been used to relate the spectral responses of the photomultiplier and Ge photodiode. To record the PL spectral distributions we used a lock-in amplifier. Lifetime measurements were excited with the dye laser described above. Coumarin 440 (or 540A) and Rhodamine 6G dyes were used for excitation of the 4S_2 and 5F_5 holmium levels, respectively. The laser pulse width has FWHM ≈ 3 ns. The nominal spectral bandwidth is ≈ 0.3 nm, but in practice the wavelength accuracy is limited to ± 1 nm by the mechanics of the tuning system. The pulsed detector signal outputs were monitored with a 500-MHz Tektronix TDS520 digital oscilloscope. In the spectroscopic experiments the sample temperature was selected in the 5–300-K temperature range by using a He closed-cycle cryostat connected to a suitable temperature controller.

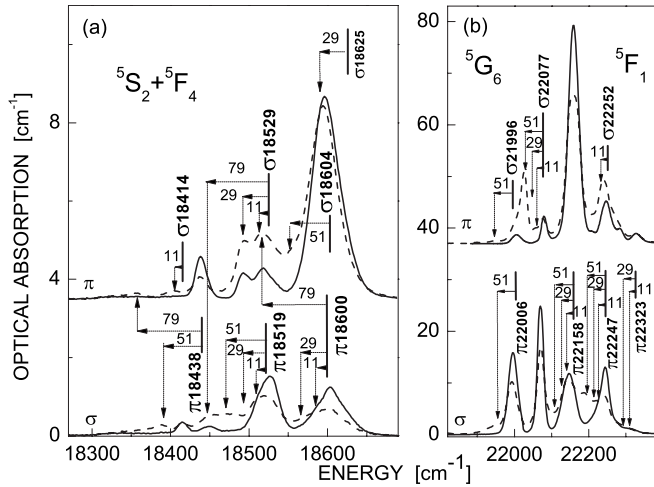


FIG. 1. Comparison of the 5-K (solid line) and 75-K (dashed line) selected optical absorption of Ho^{3+} in NaBiW. $[\text{Ho}]=0.35 \times 10^{20} \text{ cm}^{-3}$. π spectra are arbitrarily displaced in the y axis for clarity.

IV. Ho^{3+} ENERGY LEVELS

A. Low-temperature ground-state absorption and photoluminescence

Ho^{3+} energy-level positions were investigated by low-temperature optical absorption and photoluminescence measurements. The large degeneracy of the ground 5I_8 multiplet of the $4f^{10}$ configuration of Ho^{3+} , 13 Stark energy levels in the current S_4 symmetry, hampers this task. Usually $^5I_8(1)$ and $^5I_8(2)$, and sometimes even $^5I_8(3)$, excited Stark levels are only few cm^{-1} above the ground $^5I_8(0)$ (Ref. 18) level, and therefore they can be electronically populated even at 5 K, giving rise to *hot bands*, $^5I_8(n \geq 1) \rightarrow ^{2S+1}L_J$, merged together with those corresponding to true ground-state transitions, $^5I_8(0) \rightarrow ^{2S+1}L_J$. Measurements at very low temperatures ≈ 1.4 K can be thus required to fully depopulate the excited $^5I_8(n \geq 1)$ Stark levels.

To overcome this uncertainty, we have measured the optical absorption of several excited multiplets at different temperatures in the 5–75-K range. Figure 1 shows a representative example of the OA thermal evolution. It is worth noting that while the intensity of some bands in a given polarization decreases with increasing temperature, some new bands may appear in the alternative polarization but shifted to low energy. This behavior will be explained later in the framework of the transition polarization rules expected for the S_4 point symmetry. At this point we just want to note that from the systematic analysis of the energy position of the bands whose observation has been induced by raising the sample temperature we determine $^5I_8(n \geq 1)$ levels at 11, 29, and 51 cm^{-1} for Ho^{3+} in NaBiW. Similar results were achieved for Ho^{3+} in NaBiMo and LiBiMo; see Table II.

The energy positions of the $^5I_8(n)$ Stark levels have been further assessed by low-temperature PL to the ground 5I_8 multiplet. Figure 2 shows a comparison of the $^5S_2 \rightarrow ^5F_5 \rightarrow$, and $^5I_6 \rightarrow ^5I_8(n)$ emissions of Ho-doped NaBiMo taken as an example. Results for Ho-doped NaBiW were very similar,

and they are not shown for the sake of brevity, while the bands observed in Ho^{3+} -doped LiBiMo have lower resolution due to the broader bands observed and therefore led to a lower number of experimentally determined 5I_8 Stark levels [see Fig. 2(c) and Table II].

For two (5F_5 and 5I_6) of the Ho^{3+} -emitting multiplets in NaBiMo the PL shows a first set of four overlapped bands (0, 22, 49, and 72 cm^{-1}) followed by an energy gap, an isolated band (179 cm^{-1}), and finally two overlapped bands (233, 260 cm^{-1}). The photoluminescence from the 5S_2 multiplet is slightly different in terms of the relative intensity of the last three bands. This suggests that the ground $^5S_2(0)$ Stark level belongs to a different IR than those of $^5F_5(0)$ and $^5I_6(0)$.

Taking into account the possible *hot* OA bands, the relative Ho^{3+} energy-level positions in the considered Bi-based DT and DMO have been investigated by 5-K-polarized OA. The wider range of ultraviolet transparency of NaBiW allows identifying electronic transitions to multiplets up to 28 000 cm^{-1} above the ground 5I_8 multiplet—i.e., up to 3H_4 —with only the exception of 5I_4 . In NaBiMo and LiBiMo hosts the Ho^{3+} spectra are limited by the UV band edge at ~ 24 000 cm^{-1} —i.e., up to 5G_5 or a lower-energy multiplet. Moreover, the Ho^{3+} spectra in LiBiMo are less resolved as a consequence of the presence of broader bands, hampering the correct identification of hot bands, and therefore a lower number of Stark levels was determined and the polarization assignment is more uncertain. Apart from these facts the results are basically similar in the three matrices. For the sake of brevity we present in Fig. 3 only the results concerning to Ho^{3+} -doped NaBiW crystal and Table II includes the energy levels obtained for each of the three crystals. It is worth remarking that the π ($\mathbf{E} \parallel \mathbf{c}$ and $\mathbf{B} \perp \mathbf{c}$) spectra are clearly different from the σ ($\mathbf{E} \perp \mathbf{c}$ and $\mathbf{B} \parallel \mathbf{c}$) and α ($\mathbf{E} \perp \mathbf{c}$ and $\mathbf{B} \perp \mathbf{c}$) spectra; \mathbf{E} and \mathbf{B} are the electromagnetic fields and \mathbf{c} the crystal axis. The two latter spectra are very similar between them, as expected from induced electric-dipole (ED) transitions for the S_4 point symmetry discussed later.

The OA results achieved at 5 K and displayed in Figs. 1–3 do not show any resolved contribution from the two possible lattice sites or multiple host environments for Ho. Further measurements made at 1.2 K on selected multiplets showed bandwidths similar to those obtained at 5 K, and no new band structure was found. Therefore, the present energy-level sets must be understood, in each case, as corresponding to an average Ho center including the nonresolved contributions of different Ho sites and environments.

B. Crystal-field analysis and simulation of $4f^{10}$ energy levels

Although for Ln^{3+} ions with large ionic radii, like Nd and Pr, the C_2 local symmetry was required to adequately describe the $4f^N$ energy sequences and polarization behavior of transitions observed in NaBiW, NaBiMo, and LiBiMo crystals,^{24,25} the first option for a similar analysis of Ho^{3+} spectral properties must be the S_4 symmetry of T sites in the host. In fact the latter symmetry described successfully the spectroscopic properties of Er^{3+} (with ionic radii close to Ho^{3+}) in the same hosts.²⁶ In the current analysis the free-ion (FI) and crystal-field (CF) interactions have been simulta-

TABLE II. Energy levels (in cm^{-1}) of Ho^{3+} , observed at 5 K (E_o) and calculated (E_c) in S_4 symmetry for NiBiX , $X=\text{Mo}$ or W , and LiBiMo crystals. IR indicates the corresponding irreducible representation, Γ_1 , Γ_2 (σ spectra) and $\Gamma_{3,4}$ (π spectra).

| $2S+1L_J$ | IR | NaBiW | | NaBiMo | | LiBiMo | | $2S+1L_J$ | IR | NaBiW | | NaBiMo | | LiBiMo | | $2S+1L_J$ | IR | NaBiW | | NaBiMo | | LiBiMo | |
|------------|----------------|-------|-------|--------|-------|----------------|---------|----------------|----------------|-------|-------|--------|---------|----------------|----------------|----------------|----------------|----------------|-------|--------|-------|--------|-------|
| | | E_o | E_c | E_o | E_c | E_o | E_c | | | E_o | E_c | E_o | E_c | E_o | E_c | | | E_o | E_c | E_o | E_c | E_o | E_c |
| 5I_8 | $\Gamma_{3,4}$ | 0 | 3 | 0 | 1 | 0 | | 5F_5 | Γ_2 | 15416 | 15411 | 15404 | 15397 | 15398 | | $\Gamma_{3,4}$ | $\Gamma_{3,4}$ | 22247 | 22230 | 22215 | 22205 | | |
| | Γ_2 | 11 | 10 | 9 | 9 | | | | $\Gamma_{3,4}$ | | 15416 | | 15402 | | | | Γ_1 | | 22238 | 22228 | 22214 | | |
| | Γ_2 | 29 | 28 | 22 | 18 | | | | Γ_1 | 15441 | 15432 | 15426 | 15418 | 15508 | | | Γ_2 | 22252 | 22246 | | 22215 | 22221 | |
| | Γ_1 | 51 | 52 | 45 | 43 | 55 | | | Γ_1 | 15480 | 15475 | 15469 | 15462 | 15463 | | | | | | | | | |
| | Γ_1 | | 61 | | 52 | | | | $\Gamma_{3,4}$ | 15530 | 15542 | 15514 | 15523 | | 5F_1 | | Γ_1 | | 22281 | 22261 | 22253 | 22277 | |
| | $\Gamma_{3,4}$ | 79 | 76 | 72 | 64 | | | | Γ_2 | 15548 | 15552 | | 15531 | 15528 | | | | $\Gamma_{3,4}$ | 22323 | 22326 | 22308 | 22307 | |
| | Γ_1 | | 201 | 179 | 178 | 178 | | | Γ_1 | | 15561 | 15529 | 15542 | | | | | | | | | | |
| | $\Gamma_{3,4}$ | | 254 | 233 | 234 | | | | $\Gamma_{3,4}$ | 15575 | 15580 | 15559 | 15563 | 15551 | 5G_5 | | Γ_1 | 23874 | 23876 | 23860 | 23848 | 23819 | |
| | Γ_1 | | 260 | | 243 | | | | | | | | | | | | $\Gamma_{3,4}$ | 23879 | 23883 | 23838 | 23855 | 23842 | |
| | Γ_2 | 266 | 262 | 260 | 262 | 252 | 5S_2 | | Γ_2 | | 18410 | | 18395 | | | | Γ_2 | | 23905 | | 23870 | | |
| | Γ_1 | | 283 | | 259 | | | | Γ_1 | 18414 | 18413 | 18404 | 18397 | 18400 | | | Γ_2 | | 23941 | | 23907 | | |
| | $\Gamma_{3,4}$ | | 289 | | 272 | | | | $\Gamma_{3,4}$ | 18438 | 18440 | 18422 | 18422 | 18424 | | | $\Gamma_{3,4}$ | | 23944 | | 23912 | | |
| | Γ_2 | | 304 | | 272 | | | | Γ_2 | 18449 | 18448 | | 18430 | | | | Γ_1 | 23963 | 23960 | | 23928 | | |
| | | | | | | | | | | | | | | | | | $\Gamma_{3,4}$ | 23967 | 23975 | 23946 | 23946 | 23927 | |
| | | | | | | | | | | | | | | Γ_1 | 23998 | 23992 | | 23957 | 23968 | | | | |
| 5I_7 | Γ_2 | | 5130 | | 5125 | | 5F_4 | Γ_1 | | 18525 | 18508 | 18512 | 18502 | | $\Gamma_{3,4}$ | Γ_1 | 23998 | 23992 | | 23957 | 23968 | | |
| | $\Gamma_{3,4}$ | 5135 | 5135 | 5130 | 5130 | 5135 | | $\Gamma_{3,4}$ | 18519 | 18534 | | 18513 | | | | | | | | | | | |
| | Γ_2 | 5135 | 5138 | 5130 | 5131 | | | Γ_2 | 18529 | 18526 | 18513 | 18519 | | 5G_4 | | Γ_2 | | 25725 | | | | | |
| | Γ_1 | 5146 | 5144 | | 5141 | | | $\Gamma_{3,4}$ | 18600 | 18597 | 18579 | 18582 | 18571 | | | Γ_1 | 25776 | 25770 | | | | | |
| | $\Gamma_{3,4}$ | | 5160 | | 5150 | | | Γ_1 | | 18599 | | 18589 | 18581 | | | $\Gamma_{3,4}$ | 25779 | 25781 | | | | | |
| | Γ_1 | | 5182 | 5165 | 5174 | | | Γ_2 | 18604 | 18614 | 18585 | 18594 | | Γ_1 | | | 25829 | | | | | | |
| | $\Gamma_{3,4}$ | 5205 | 5202 | 5193 | 5192 | 5188 | | Γ_1 | 18625 | 18625 | 18605 | 18608 | | $\Gamma_{3,4}$ | | 25825 | 25836 | | | | | | |
| | Γ_2 | | 5207 | 5201 | 5198 | | | | | | | | | | | Γ_2 | 25850 | 25863 | | | | | |
| | $\Gamma_{3,4}$ | 5264 | 5267 | 5255 | 5258 | | | 5F_3 | $\Gamma_{3,4}$ | 20562 | 20550 | 20547 | 20538 | 20531 | | | Γ_1 | 25914 | 25891 | | | | |
| | Γ_2 | 5265 | 5265 | 5255 | 5260 | 5258 | | | Γ_1 | 20577 | 20571 | 20564 | 20556 | 20545 | | | | | | | | | |
| Γ_1 | | 5268 | | 5261 | | Γ_2 | 20621 | | 20615 | 20606 | 20598 | 20605 | 3K_7 | $\Gamma_{3,4}$ | | 26125 | | | | | | | |
| | | | | | | $\Gamma_{3,4}$ | 20672 | | 20669 | 20655 | 20653 | 20637 | | Γ_2 | | 26126 | | | | | | | |
| 5I_6 | Γ_1 | | 8651 | | 8651 | | 5F_2 | Γ_2 | 20666 | 20668 | 20645 | 20653 | | | Γ_1 | | 26127 | | | | | | |
| | Γ_2 | 8656 | 8651 | | 8651 | | | | | | | | | Γ_2 | 26145 | 26143 | | | | | | | |
| | $\Gamma_{3,4}$ | | 8657 | | 8654 | | | Γ_2 | | 21043 | | 21034 | | | $\Gamma_{3,4}$ | 26151 | 26137 | | | | | | |
| | Γ_2 | 8665 | 8663 | | 8657 | | | Γ_1 | 21046 | 21046 | 21035 | 21035 | 21032 | | Γ_1 | | 26166 | | | | | | |
| | $\Gamma_{3,4}$ | 8667 | 8664 | 8662 | 8664 | 8659 | | $\Gamma_{3,4}$ | 21085 | 21085 | 21073 | 21073 | 21058 | | $\Gamma_{3,4}$ | | 26172 | | | | | | |
| | Γ_1 | | 8673 | | 8670 | | | Γ_2 | 21137 | 21138 | 21120 | 21126 | 21114 | | Γ_1 | | 26176 | | | | | | |
| | Γ_2 | 8677 | 8677 | | 8673 | 8676 | | | | | | | | | $\Gamma_{3,4}$ | 26179 | 26185 | | | | | | |
| | Γ_1 | | 8752 | | 8751 | | | 3K_8 | Γ_1 | 21327 | 21321 | 21321 | 21316 | | | Γ_2 | 26180 | 26182 | | | | | |

TABLE II. (Continued.)

| $^{2S+1}L_J$ | IR | NaBiW | | NaBiMo | | LiBiMo | $^{2S+1}L_J$ | IR | NaBiW | | NaBiMo | | LiBiMo | $^{2S+1}L_J$ | IR | NaBiW | | NaBiMo | | LiBiMo |
|--------------|----------------|-------|-------|--------|-------|--------|--------------|----------------|-------|-------|--------|-------|--------|--------------|----------------|------------|-------|--------|-------|--------|
| | | E_o | E_c | E_o | E_c | E_o | | | E_o | E_c | E_o | E_c | E_o | | | E_c | E_o | E_o | E_c | E_o |
| 5I_5 | $\Gamma_{3,4}$ | 8761 | 8763 | 8762 | 8759 | 8744 | | Γ_2 | 21327 | 21324 | 21321 | 21320 | 21318 | | Γ_2 | | 26186 | | | |
| | Γ_2 | | 8773 | | 8768 | | | $\Gamma_{3,4}$ | 21331 | 21329 | 21323 | 21324 | | | | | | | | |
| | | | | | | | | Γ_1 | | 21338 | | 21329 | | | 5G_5 | Γ_2 | 27484 | 27495 | | |
| | $\Gamma_{3,4}$ | | 11215 | | 11208 | | | $\Gamma_{3,4}$ | 21341 | 21340 | | 21333 | | | $\Gamma_{3,4}$ | 27507 | 27502 | | | |
| | Γ_1 | | 11217 | | 11212 | | | Γ_2 | | 21340 | 21329 | 21330 | | | Γ_1 | 27507 | 27516 | | | |
| | $\Gamma_{3,4}$ | 11224 | 11220 | | 11220 | | | Γ_1 | | 21362 | | 21352 | | | Γ_1 | 27583 | 27590 | | | |
| | Γ_1 | | 11224 | | 11219 | | | $\Gamma_{3,4}$ | 21400 | 21411 | 21390 | 21396 | | | $\Gamma_{3,4}$ | 27585 | 27574 | | | |
| | Γ_2 | | 11226 | | 11226 | | | Γ_1 | | 21412 | | 21397 | | | Γ_2 | 27635 | 27629 | | | |
| | Γ_1 | | 11284 | | 11285 | | | Γ_1 | | 21414 | | 21399 | 21400 | | $\Gamma_{3,4}$ | 27653 | 27629 | | | |
| | $\Gamma_{3,4}$ | 11286 | 11306 | | 11301 | | | Γ_2 | 21423 | 21431 | 21410 | 21415 | 21412 | | Γ_1 | | 27632 | | | |
| 5I_4 | Γ_2 | | 11310 | | 11305 | | | $\Gamma_{3,4}$ | 21441 | 21437 | 21428 | 21419 | | | | | | | | |
| | | | | | | | | Γ_2 | 21437 | 21438 | | 21419 | | | $^5H(4)_6$ | Γ_1 | 27728 | 27733 | | |
| | Γ_1 | | 13170 | | 13180 | | | | | | | | | | Γ_2 | | 27738 | | | |
| | $\Gamma_{3,4}$ | | 13240 | | 13243 | | 5G_6 | Γ_2 | 21996 | 22007 | 21980 | 21988 | 21963 | | $\Gamma_{3,4}$ | 27756 | 27750 | | | |
| | Γ_2 | | 13292 | | 13296 | | | $\Gamma_{3,4}$ | 22006 | 22015 | 21982 | 21994 | | | Γ_2 | 27771 | 27780 | | | |
| | Γ_1 | | 13307 | | 13297 | | | Γ_1 | | 22026 | | 22005 | | | $\Gamma_{3,4}$ | 27865 | 27846 | | | |
| | Γ_2 | | 13333 | | 13329 | | | Γ_2 | 22077 | 22082 | 22056 | 22057 | 22047 | | Γ_2 | | 27846 | | | |
| | $\Gamma_{3,4}$ | | 13384 | | 13382 | | | Γ_2 | | 22083 | | 22058 | | | Γ_1 | | 27866 | | | |
| | Γ_1 | | 13494 | | 13477 | | | Γ_1 | 22155 | 22156 | | 22132 | | | Γ_1 | | 27874 | | | |
| | | | | | | | | $\Gamma_{3,4}$ | 22158 | 22155 | 22133 | 22130 | 22118 | | $\Gamma_{3,4}$ | 27897 | 27910 | | | |
| | | | | | | | | | | | | | | Γ_2 | 27918 | 27927 | | | | |

174208-5

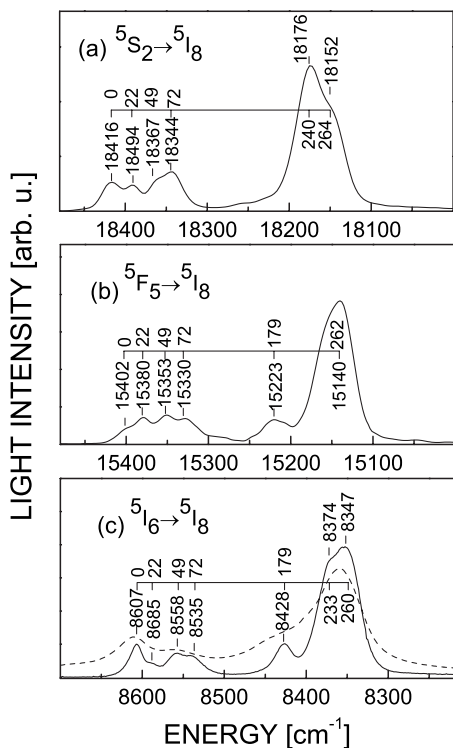


FIG. 2. 5-K $^{2S+1}L_J \rightarrow ^5I_8$ unpolarized photoluminescence of Ho^{3+} in NaBiMo (solid line) and in LiBiMo (dashed line).

neously considered in the procedure of fitting the observed energy levels. In this manner all intermediate coupling and crystal-field J -mixing effects are included in the calculations and arbitrary adjustments of the barycenter of the multiplets have been avoided. The theoretical background, including the expressions of the corresponding FI and CF Hamiltonians, and a short description of the IMAGE routine used to perform the current CF analysis, can be found in Ref. 27.

For the S_4 symmetry of Ho^{3+} in MBiX hosts the CF potential involves five real B_q^k and one complex S_q^k parameters (after setting S_4^4 to zero by choosing adequate reference axes for the system), which must be adjusted to give the best agreement between the calculated and observed Stark levels. These levels are characterized by the IR of the S_4 point group, monodimensional, Γ_1 , Γ_2 , or bidimensional, $\Gamma_{3,4}$. The selection rules for induced ED or magnetic dipolar (MD) transitions for S_4 symmetry and an even number of electrons are collected in Table III. Since the $4f^{10}$ configuration does not include any nondegenerate excited state, the attribution of the IR for the $^5I_8(0)$ ground level is not straightforward. To proceed with this analysis we have first simulated the sequence of the Ho^{3+} energy levels using the previously reported CF parameters of Er^{3+} in NaBiW²⁶ and FI parameters calculated for Ho^{3+} in monoclinic $\text{KGd}(\text{WO}_4)_2$ α -KGW.²⁸ In the calculation process, the S_4 $4f^{10}$ states—i.e., the observed energy levels—are distributed in three submatrices, each being a submatrix associated with only one IR. These matrices contain 257, 254, and 245 energy levels, and consequently the last one will correspond to the IR $\Gamma_{3,4}$. This initial simulation showed that $^5I_8(0)$ belongs to IR $\Gamma_{3,4}$, in agreement with the results found for Ho^{3+} in the closely related CaWO_4

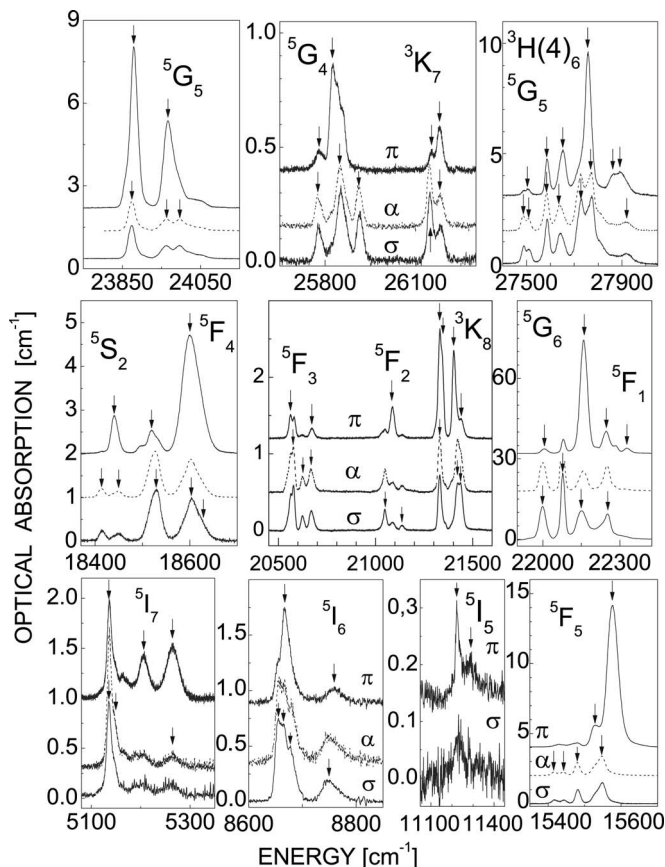


FIG. 3. Polarized 5-K optical absorption of Ho^{3+} in NaBiMo single crystal. $[\text{Ho}] = 0.35 \times 10^{20} \text{ cm}^{-3}$. The arrows indicate transitions considered as starting in $^5I_8(0)$.

crystal,²⁹ while $^5I_8(1)$ and $^5I_8(2)$ correspond to the same IR, either Γ_1 or Γ_2 , and $^5I_8(3)$, which appears in the remaining submatrix, to the other IR—that is, Γ_2 or Γ_1 .

Once the IR of the ground level was assessed, we assigned the excited ones as Γ_1 or Γ_2 if the corresponding band appears in the σ (or α) spectrum or as $\Gamma_{3,4}$ when the band appears in the π spectrum. Finally, the Γ_1 and Γ_2 assignment was made on the basis of the best adjustment to the calculated energy levels in the corresponding submatrices, which sometimes only differs in a few cm^{-1} —that is, inside the experimental error of the Ho^{3+} bands. Current fits indicate that for the NaBiW host the observed $^5I_8(1)$ and $^5I_8(2)$ levels, at 11 and 29 cm^{-1} , are Γ_2 singlets, which once again agrees with the energy and IR found for Ho^{3+} levels in CaWO_4 ,³⁰ and in the also scheelite-type LiYF_4 crystals,³¹ while $^5I_8(3)$, at 51 cm^{-1} , corresponds to Γ_1 . The thermal OA

TABLE III. Selection rules for ED and MD transitions for S_4 symmetry and an even number of f electrons.

| | ED | | | MD | | |
|----------------|------------------|------------------|------------------|---------------|---------------|----------------|
| | Γ_1 | Γ_2 | $\Gamma_{3,4}$ | Γ_1 | Γ_2 | $\Gamma_{3,4}$ |
| Γ_1 | | π | α, σ | σ | | σ, π |
| Γ_2 | π | | α, σ | | σ | σ, π |
| $\Gamma_{3,4}$ | α, σ | α, σ | π | σ, π | σ, π | σ |

behavior presented in Fig. 1 can now be rationalized: Transitions to a given excited Stark level and starting from ${}^5I_8(1,2,3)$ levels must appear either in a different polarization than that observed when starting from the ${}^5I_8(0)$ or become forbidden.

The optical absorption of Ho^{3+} in NaBiW, NaBiMo, and LiBiMo was basically identical for α and σ spectra; therefore, the intensity of the observed transitions is dominated by the induced ED contribution, even for those with $\Delta J=1$, which have non-negligible MD contributions.³² For the present analysis we have assigned each band to the polarization where it is observed with higher intensity, although often a residual intensity is also observed in the other polarization configuration. It must be noted that several centers associated with the two independent $2b$ and $2d$ lattice sites for $T=\text{Ho}^{3+}$, as well as with different Na (or Li) and Bi environments around both sites, are simultaneously contributing to the experimental spectra. This is the likely reason for the residual contributions described above, and the present energy levels must be understood as corresponding to an average Ho^{3+} center.

The CF calculation was done first for Ho^{3+} in NaBiW because of the larger number of observed energy levels. The total Hamiltonian includes 26 parameters, and among them some FI parameters have been held constant through the adjustment, while others were constrained to vary within determined ratios. The results achieved in NaBiW were taken as the model for the IR and submatrix assignments of Ho^{3+} in NaBiMo. The values of the Judd parameters, initially those obtained for NaBiW, after a few cycles of refinement were kept constant along the adjustment process.

In both hosts and despite the modest number of observed Stark levels, the simulation reproduces very adequately the experimental Ho^{3+} -NaBiW and NaBiMo level sequences, with overall agreements of $\sigma=8.8$ and 7.3 cm^{-1} , respectively, and in no case have large individual discrepancies between experimental and calculated energy levels been found; see Table II. These uncertainties are small considering the precision of the experimental data inherent to the large linewidth. The final results of the refinements are summarized in Table II, for the energy levels, and in Table IV, for adjusted FI and CF parameters. EPAPS MS Word Supplementary Documents with calculated energy levels of the Ho^{3+} configuration in $\text{NaBi}(\text{WO}_4)_2$ and in $\text{NaBi}(\text{MoO}_4)_2$, indicating the three main components of their corresponding associated wave functions, up to ${}^3H(4)_6$, $\sim 28\,000 \text{ cm}^{-1}$ and 5G_5 , $\sim 24\,000 \text{ cm}^{-1}$, respectively, are available.²⁷ Lists of energy levels in these configurations up to $60\,000 \text{ cm}^{-1}$ can be also obtained from the authors. The confidence in the obtained phenomenological parameters and the physical meaning of the fits are supported not only by the low σ values obtained, but also by the very similar results of previous calculations performed either independently for the same $4f^{10} \text{Ho}^{3+}$ configuration in the isostructural scheelite CaWO_4 crystal³⁰ or those parallel for the closest $4f^{11} \text{Er}^{3+}$ configuration in the same crystalline matrices,²⁶ which provide S_4 CF parameter sets with only smooth variations.

V. Ho^{3+} RADIATIVE PROCESSES

Ho^{3+} has a large number of electronic transitions which can lead to laser action.¹⁸ The most important ones are those

TABLE IV. Free-ion and CF parameters (cm^{-1}) in S_4 symmetry for Ho^{3+} in $\text{NaBi}(\text{XO}_4)_2$, $X=\text{W}, \text{Mo}$, single crystals. Values in parentheses refer to estimate standard deviations in the indicated parameter. Values in square brackets were not allowed to vary in the parameter fitting.

| | NaBiW | NaBiMo |
|-----------------------|---------------|---------------|
| E^0 | 47647.9(9) | 47624.2(9) |
| E^2 | 6381.6(3) | 6390.0(3) |
| E^4 | 31.78(2) | 31.92(3) |
| E^6 | 637.33(5) | 633.26(6) |
| α | 17.37(3) | 16.60 |
| β | -670(2) | -729(1) |
| γ | [1750] | [1750] |
| ζ | 2140.5(5) | 2148.9(5) |
| M^0 ^a | 3.5(6) | [3.5] |
| P^2 ^b | 750(20) | [825] |
| T^2 | [330] | [330] |
| T^3 | 37(2) | [38] |
| T^4 | 112(2) | [172] |
| T^6 | -197(10) | [-127] |
| T^7 | 237(22) | [336] |
| T^8 | [336] | [336] |
| B_0^2 | 411(31) | 440(30) |
| B_0^4 | -601(30) | -565(34) |
| B_4^4 | $\pm 832(18)$ | $\pm 800(21)$ |
| B_0^6 | -67(34) | -54(32) |
| B_4^6 | $\pm 576(20)$ | $\pm 509(19)$ |
| S_4^6 | $\pm 195(54)$ | $\pm 85(42)$ |
| S_2^c | 184 | 197 |
| S_4 | 440 | 422 |
| S_6 | 239 | 203 |
| S_T | 308 | 293 |
| L | 85 | 56 |
| σ ^d | 8.8 | 7.3 |
| Residue | 5289.2 | 2296.5 |

^a $M^0 M^2=0.56M^0$, $M^4=0.32M^0$.

^b $P^4=0.75P^2$, $P^6=0.50P^2$.

^cThe crystal field strength parameters S_T and S_K are defined (Ref. 33) as $S_T=[\frac{1}{3}\sum_k S_k^2]^{1/2}$, $S_K=\{[\frac{1}{2k+1}[(B_0^k)^2+2\sum_q[(B_q^k)^2+(S_q^k)^2]]]^{1/2}$.

^d $\sigma=[\sum(\Delta_i)^2/(L-P)]^{1/2}$, $\Delta_i=E_i-E_c$, L number of levels, P number of parameters.

operating at room temperature and related to deexcitations from three different multiplets: ${}^5I_6 \rightarrow {}^5I_7$ ($\lambda=3 \mu\text{m}$), ${}^5I_7 \rightarrow {}^5I_8$ ($\lambda=2 \mu\text{m}$), and ${}^5S_2 \rightarrow {}^5I_7$ ($\lambda=760 \text{ nm}$), $\rightarrow {}^5I_6$ ($\lambda=1.03 \mu\text{m}$), $\rightarrow {}^5I_5$ ($\lambda=1.4 \mu\text{m}$), and $\rightarrow {}^5F_5$ ($\lambda=3.37 \mu\text{m}$). Moreover, the ${}^5F_5 \rightarrow {}^5I_{5,6,7}$ deexcitations produce laser operation at cryogenic temperatures and the ${}^5I_5 \rightarrow {}^5I_6$ ($\lambda=3.9 \mu\text{m}$) has been also reported in selected systems. In this section we study first the expected radiative properties of Ho^{3+} in the considered Bi-based DT and DMo, and later we show the actual properties as a function of the temperature and concentration, with particular emphasis on the above-mentioned laser-related multiplets.

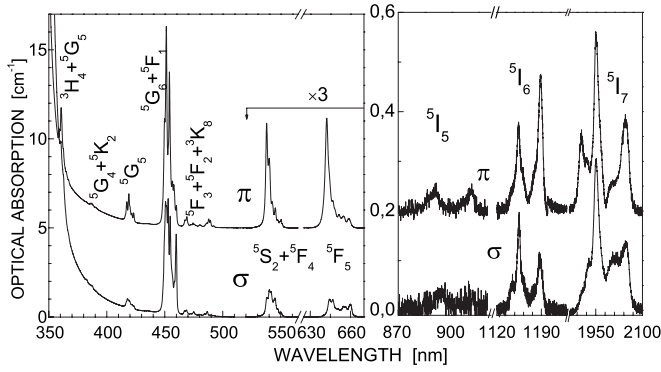


FIG. 4. 300-K ground state ($^5I_8 \rightarrow ^{2S+1}L_J$) optical absorption of Ho^{3+} in NaBiW single crystal. $[\text{Ho}]_{\text{cryst}} = 0.35 \times 10^{20} \text{ cm}^{-3}$.

A. Judd-Ofelt calculations

The Judd-Ofelt (JO) theory^{34,35} is often used to obtain the radiative properties of $4f$ transitions of Ln^{3+} in solid and liquid hosts. The theory uses 300-K integrated absorption cross sections $[\text{Ho}]^{-1} \int \alpha d\lambda$ to calculate the JO parameters Ω_k ($k=2, 4, 6$), from which radiative transition rates $A_{JJ'}$, luminescence branching ratios $\beta_{JJ'} = A_{JJ'} / \sum_{J'} A_{JJ'}$, and radiative lifetimes $\tau_{r,J} = 1 / \sum_{J'} A_{JJ'}$ for each J manifold can be achieved. Details of the JO treatment and definitions can be found in previous works.^{28,34,35}

To perform these calculations we measured the room-temperature polarized OA of Ho^{3+} in the three considered Bi-based DT and DMO crystal hosts. Figure 4 shows the

results obtained in Ho-doped NaBiW. For Ho-doped NaBiMo and LiBiMo crystals the spectra (not shown for the sake of brevity) were similar to those shown in Fig. 4 but a lower number of transitions were determined due to the smaller energy gap of the molybdate hosts. Table V summarizes the experimental integrated cross sections, which were weighted as $(2\sigma + \pi)/3$ to obtain the experimental oscillator strengths \bar{f}_o . In this process the refractive index values of each matrix at the corresponding average wavelength were considered.^{4,16}

The JO Ω_k parameter sets obtained for the two molybdate hosts are very similar but slightly different from that obtained for the tungstate host. In particular, the Ω_4 parameter in NaBiW is significantly larger. Ω_2 is mainly determined by the $^5I_8 \rightarrow ^5G_6$ transition probability which is rather similar in the three hosts. Ω_4 is determined by the $^5I_8 \rightarrow ^5F_5$, 5F_4 , and 5G_6 transition probability; therefore, the Ω_4 difference between NaBiW and Na(Li)BiMo is related to the larger absorption cross section of the 5F_5 and 5F_4 multiplets in the latter host, particularly for the π contribution. All the Ω_k sets obtained are within the usual values found for Ho^{3+} in solids.³² In particular they agree rather well with those reported for Ho^{3+} in the NaYMo,³⁶ but are clearly different from those reported for Ho:NaYW.³⁷ Our analysis is later validated by a comparison of the calculated spectroscopic magnitudes with the experimental results.

The radiative properties obtained by using the Ω_k set for each host are summarized in Table VI for transitions with fluorescence branching ratios larger than $\approx 20\%$ and, when possible, compared with experimental results. Magnetic-

TABLE V. Room-temperature spectroscopic absorbance properties of Ho^{3+} in NaBiW, NaBiMo, and LiBiMo crystals. σ - and π -polarized integrated ground state ($^5I_8 \rightarrow ^{2S+1}L_J$) absorption cross section, $\int \sigma = [\text{Ho}]^{-1} \int \alpha d\lambda$. $\bar{\lambda}$ is the corresponding average wavelength of each $^{2S+1}L_J$ multiplet. Observed oscillator strength (\bar{f}_o), calculated electric-dipole oscillator strength (f_{ED}), $|\Delta f| = |\bar{f}_o - f_{\text{ED}}|$, JO parameters Ω_k ($\times 10^{-20} \text{ cm}^2$).

| | NaBiW | | | | | | NaBiMo | | | | | | LiBiMo | | | | | | |
|-------------------------|---------------|------------|-----------------|--------------------|-----------------|--------------|---------------|------------|-----------------|----------------------|-----------------|--------------|---------------|------------|-----------------|----------------------|-----------------|--------------|--|
| $^5I_8 \rightarrow$ | $\int \sigma$ | $\int \pi$ | $\bar{\lambda}$ | \bar{f}_o | f_{ED} | $ \Delta f $ | $\int \sigma$ | $\int \pi$ | $\bar{\lambda}$ | \bar{f}_o | f_{ED} | $ \Delta f $ | $\int \sigma$ | $\int \pi$ | $\bar{\lambda}$ | \bar{f}_o | f_{ED} | $ \Delta f $ | |
| $^3H(4)_6$ | 100 | 170 | 361 | 1066 | 1494 | 428 | | | | | | | | | | | | | |
| $^3K_7 + ^5G_4$ | 17 | 18 | 388 | 132 | 135 | 3 | | | | | | | | | | | | | |
| 5G_5 | 145 | 66 | 419 | 764 | 209 | 555 | | | | | | | | | | | | | |
| $^5G_6 + ^5F_1$ | 1279 | 1390 | 453 | 7247 | 7203 | 44 | 1062 | 1465 | 453 | 6589 | 6589 | 0 | 1286 | 1674 | 453 | 7976 | 7976 | 0 | |
| $^5F_3 + ^5F_2 + ^3K_8$ | 64 | 114 | 478 | 402 | 259 | 143 | 56 | 73 | 478 | 306 | 210 | 96 | 68 | 89 | 477 | 371 | 271 | 100 | |
| $^5F_4 + ^5S_2$ | 115 | 261 | 541 | 632 | 497 | 135 | 86 | 130 | 541 | 387 | 307 | 80 | 104 | 158 | 542 | 469 | 383 | 86 | |
| 5F_5 | 111 | 209 | 648 | 478 | 575 | 97 | 90 | 161 | 648 | 304 | 326 | 22 | 109 | 195 | 649 | 368 | 391 | 23 | |
| 5I_5 | 16 | 16 | 899 | 22 | 17 | 5 | 5 | 8 | 899 | 13 | 19 | 6 | | | | | | | |
| 5I_6 | 96 | 142 | 1170 | 94 | 82 | 12 | 65 | 106 | 1165 | 66 | 60 | 6 | 105 | 113 | 1165 | 90 | 77 | 13 | |
| 5I_7 | 514 | 568 | 1960 | 91 | 129 | 38 | 413 | 585 | 1960 | 71 | 91 | 20 | 539 | 605 | 1960 | 93 | 116 | 23 | |
| f_{MD}^a | | | | +65.2 | | | | | | +67.2 | | | | | | +71.2 | | | |
| Ω_2 | | | | 10.5 | | | | | | 9.5 | | | | | | 10.1 | | | |
| Ω_4 | | | | 5.2 | | | | | | 2.6 | | | | | | 2.7 | | | |
| Ω_6 | | | | 0.6 | | | | | | 0.4 | | | | | | 0.5 | | | |
| rms | | | | 2×10^{-6} | | | | | | 0.7×10^{-6} | | | | | | 0.8×10^{-6} | | | |

^aThe magnetic-dipole f_{MD} contribution has been discounted from the 5I_7 experimental oscillator strength to obtain the reported observed \bar{f}_o value.

TABLE VI. Radiative properties of Ho^{3+} in NaBiW, NaBiMo, and LiBiMo crystals. Total electric-dipole, ED, plus magnetic-dipole, MD (in parentheses) radiative transitions rates $A_{JJ'}$. Calculated and 300 K observed branching ratios $\beta_{JJ'}$, β_o (in parentheses). Radiative, τ_r , and 5 K observed τ_o , lifetimes. The observed branching ratios and lifetimes were measured in samples with low ($<1 \times 10^{19} \text{ cm}^{-3}$) Ho concentration.

| | λ [nm] | NaBiW | | | NaBiMo | | | LiBiMo | | |
|---------------------------|-------------------|----------------------------------|------------------------------------|--|----------------------------------|------------------------------------|--|----------------------------------|------------------------------------|--|
| | | $A_{JJ'}$ [s^{-1}] | $\beta_{JJ'}$ (β_o) [%] | τ_r (τ_o) [μs] | $A_{JJ'}$ [s^{-1}] | $\beta_{JJ'}$ (β_o) [%] | τ_r (τ_o) [μs] | $A_{JJ'}$ [s^{-1}] | $\beta_{JJ'}$ (β_o) [%] | τ_r (τ_o) [μs] |
| $^3K_7 \rightarrow ^5I_7$ | 477 | 526 | 21 | 403 | | | | | | |
| 5I_8 | 385 | 1379 | 56 | | | | | | | |
| $^5G_4 \rightarrow ^5I_5$ | 583 | 35321 | 52 | 15 | | | | | | |
| 5I_7 | 484 | 14049 | 21 | | | | | | | |
| $^5G_5 \rightarrow ^5I_7$ | 534 | 34253 | 69 | 20 | 36586 | 75 | 20 | 44212 | 74 | 17 |
| $^5F_1 \rightarrow ^5I_4$ | 1115 | 1310 | 24 | 181 | 734 | 20 | 277 | 852 | 19 | 223 |
| 5I_5 | 903 | 2792 | 50 | | 1656 | 46 | | 1972 | 44 | |
| | | | | | 760 | 21 | | 1010 | 23 | |
| $^5G_6 \rightarrow ^5I_8$ | 455 | 156444 | 94 | 6 | 161136 | 95 | 6 | 197868 | 95 | 5 |
| $^3K_8 \rightarrow ^5I_8$ | 472 | 2475 | 91 | 369 | 2253 | 92 | 408 | 2806 | 92 | 328 |
| $^5F_2 \rightarrow ^5I_6$ | 807 | 2178 | 39 | 180 | 1309 | 33 | 250 | 1562 | 31 | 196 |
| 5I_8 | 478 | 1818 | 33 | | 1657 | 41 | | 2258 | 44 | |
| $^5F_3 \rightarrow ^5I_7$ | 650 | 5872 | 56 | 96 | 3554 | 51 | 142 | 4244 | 49 | 115 |
| 5I_8 | 490 | 2148 | 21 | | 1960 | 28 | | 2664 | 31 | |
| $^5F_4 \rightarrow ^5I_8$ | 548 | 9430 | 73 | 77 | 6448 | 75 | 116 | 7974 | 76 | 95 |
| $^5S_2 \rightarrow ^5I_6$ | 1010 | 864 | 11 (14) | 381 (16) | 183 | 9 (12) | 469 (12) | 228 | 20 (8) | 353 (11) |
| 5I_7 | 746 | 278 | 33 (34) | | 701 | 33 (27) | | 931 | 33 (33) | |
| 5I_8 | 543 | 1372 | 52 (51) | | 1173 | 55 (61) | | 1578 | 56 (46) | |
| $^5F_5 \rightarrow ^5I_6$ | 1456 | 214 | 3 (12) | 117 (1.9) | 148 | 3 | 189 (2.0) | 180 | 3 | 157 (1.7) |
| 5I_7 | 965 | 1605 | 19 (28) | | 1017 | 19 (38) | | 1210 | 19 (39) | |
| 5I_8 | 650 | 6699 | 78 (60) | | 4120 | 78 (62) | | 4952 | 78 (60) | |
| $^5I_4 \rightarrow ^5I_6$ | 2151 | 42 | 39 | 9084 | 33 | 38 | 11524 | 42 | 38 | 9084 |
| 5I_7 | 1227 | 46 | 42 | | 36 | 42 | | 47 | 43 | |
| $^5I_5 \rightarrow ^5I_7$ | 1657 | 92 | 36 | 3857 | 73 | 31 | 4280 | 93 | 32 | 3465 |
| 5I_8 | 905 | 144 | 55 | | 140 | 60 | | 172 | 60 | |
| $^5I_6 \rightarrow ^5I_7$ | 2860 | (30) 65 | 22 | 3345 | (32) 56 | 24 | 4225 | (34) 63 | 22 | 3437 |
| 5I_8 | 1174 | 234 | 78 | | 180 | 76 | | 227 | 78 | |
| $^5I_7 \rightarrow ^5I_8$ | 1993 | (57) 165 | 100 | 6047 | (60) 141 | 100 | 7089 | (77) 178 | 100 | 5613 |

dipole contributions have been explicitly considered when needed. These contributions are particularly relevant for the $^5I_6 \rightarrow ^5I_7$ ($\lambda=3 \mu\text{m}$) and $^5I_7 \rightarrow ^5I_8$ ($\lambda=2 \mu\text{m}$) laser transitions with $\Delta J=1$. The uncertainty of the radiative JO magnitudes obtained is estimated about $\pm 15\%$ due mainly to the experimental uncertainty in the measurement of the Ho concentration. Within this uncertainty, the Ho^{3+} radiative results obtained for the three hosts must be considered as similar.

B. Ho^{3+} fluorescence

The Ho^{3+} fluorescence has been studied in several spectral ranges to evaluate the observed branching ratios β_o of corresponding multiplets as a test for JO radiative results. Figure 5 shows the fluorescence obtained for Ho-doped NaBiW. Again, the results obtained for Ho-doped NaBiMo and LiBiMo were very similar, and therefore they are not shown

for brevity. The β_o results are included in Table VI.

Due to the considerable number of possible electronic transitions in Ho^{3+} and the large energy of the excited multiplets, an overlap of emissions from several multiplets is possible. For instance, in the 1000–1030-nm emission range contributions from $^5F_2 \rightarrow ^5I_5$, $^5F_4 \rightarrow ^5I_6$, and $^5S_2 \rightarrow ^5I_6$ can be found. However, for the 5F_5 and 5S_2 fluorescence spectra shown in Fig. 5 these possible contributions are weak and correspond to transitions with small branching ratios; therefore, the observed branching ratios summarized in Table VI are a good approximation. The general agreement between the observed and calculated branching ratios of the 5S_2 and 5F_5 multiplets shows the correctness of the radiative calculations in Table VI. In particular, the $^5S_2 \rightarrow ^5I_5$, 5F_5 emissions were not observed, what agrees with the very low branching ratios obtained for these transitions.

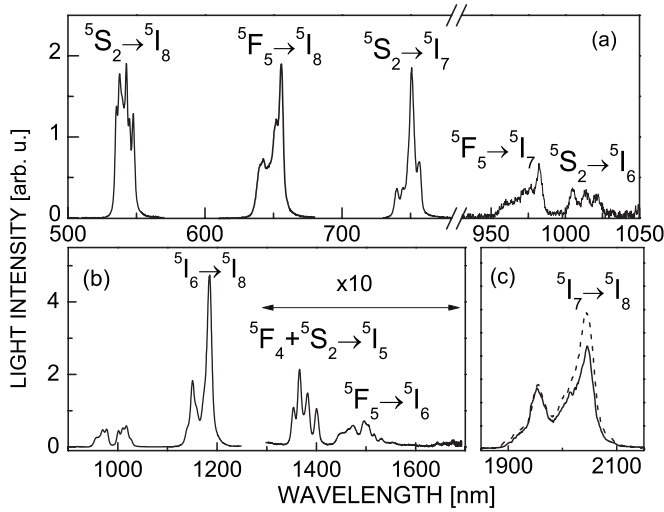


FIG. 5. 300-K fluorescence of Ho^{3+} in NaBiW. (a) Unpolarized fluorescence, $\lambda_{\text{exc}}=454$ nm ($^5G_6 + ^5F_1$). (b) Unpolarized fluorescence, $\lambda_{\text{exc}}=488$ nm (5F_3). (c) π -polarized (dashed line) and σ -polarized (solid line) fluorescences, $\lambda_{\text{exc}}=488$ nm (5F_3).

C. Ho^{3+} lifetimes

Lifetime measurements of Ln^{3+} in DT and DMo crystals have been most commonly provided in samples prepared for laser demonstration and, therefore, with a large concentration of active ions, typically above 1 at. % in the crystal. These measurements are difficult to compare with the radiative lifetime calculated by the JO analysis because several nonradiative deexcitation mechanisms coexist. In this work, as well as in our previous ones related to Nd, Pr, and Er in the same DT and DMo, we considered first samples with very low Ln^{3+} concentration for which Ln-Ln interactions can be ignored, and later on we studied these Ln-Ln interactions using samples with increasing Ln^{3+} concentration.

The Ho^{3+} lifetime results obtained in the three DT and DMo hosts here considered were similar; therefore, we shall describe the methodology and results for NaBiW and refer to Table VI for the minor differences found for Ho-doped NaBiMo and LiBiMo.

For each host we used first the sample with lowest Ho concentration; see Table I. All fluorescence intensity decays observed at this doping level ($\approx 5-7 \times 10^{18} \text{ cm}^{-3}$) were single exponential. This shows that the influence of the crystalline disorder on the energy levels is not very strong and the average centre assumption used in Sec. IV A is also valid to describe the emission properties. Figure 6(a) shows examples for the Ho-doped NaBiW sample. The multiplet 5G_6 is convenient for excitation of the 5S_2 photoluminescence because of its strong absorption; however, the large radiative lifetime of the intermediate 3K_8 multiplet can *a priori* introduce uncertainty in the measurements. To be sure that our measurements were free of this uncertainty, we compared the fluorescence intensity decays exciting at 5G_6 and 5F_4 multiplets at 300 K and 5 K. The 5S_2 lifetime obtained was independent of the excitation; therefore, we excited at the 5G_6 multiplet, which provided very intense 5S_2 fluorescence signals. This result is also consistent with the low-energy gap

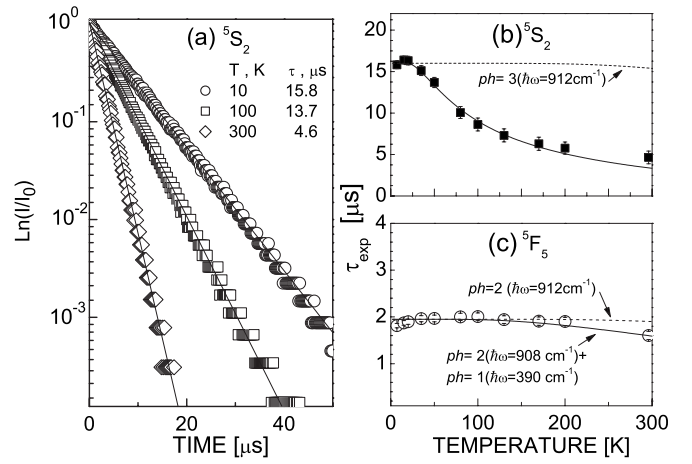


FIG. 6. Lifetimes of 5S_2 and 5F_5 levels of Ho^{3+} in NaBiW. $[\text{Ho}]=0.07 \times 10^{20} \text{ cm}^{-3}$. (a) Light intensity $^5S_2 \rightarrow ^5I_8$ decays ($\lambda_{\text{exc}}=455$ nm, $\lambda_{\text{emi}}=550$ nm) at several temperatures (points) and fits to a single-exponential law (lines). (b) Temperature dependence of the 5S_2 experimental lifetime (points), fit to a multiphonon model [Eq. (3)] (dashed line) and fit taking into account Eq. (4) (solid line). (c) Temperature dependence of the 5F_5 ($\lambda_{\text{exc}}=650$ nm, $\lambda_{\text{emi}}=660$ nm) experimental lifetime (points) and fit to the multiphonon model [Eq. (3)] (line).

between 3K_8 and 5F_2 multiplets ($<200 \text{ cm}^{-1}$); therefore, the actual 3K_8 lifetime must be shorter than the calculated radiative lifetime.

At 5 K the experimental $^5S_2 \rightarrow ^5I_8$ lifetime found in Ho-doped NaBiW was $\tau_0=16 \mu\text{s}$ (see Table VI for other hosts) and this decreased up to $\tau_0=4.6 \mu\text{s}$ at 300 K. Figure 6(b) shows the thermal dependence. It must be first noted that $\tau_0(10 \text{ K})$ of 5S_2 is much lower than the calculated radiative lifetime $\tau_r=381 \mu\text{s}$. Ho-Ho energy transfer can be ignored at such low doping concentration because of the large average Ho-Ho distance $\bar{r}=(4\pi[\text{Ho}]/3)^{-1/3} \geq 320$ nm, and since phonon emission is also minimized at 5 K, the difference between the experimental and radiative lifetimes must be ascribed to a Ho-host nonradiative interaction.

The 5F_5 lifetime in the different hosts was excited resonantly ($^5I_8 \leftrightarrow ^5F_5$) at $\lambda_{\text{exc}}=650$ nm and monitored at $\lambda_{\text{emi}}=660$ nm. Procedures similar to the case above and the same low-concentrated samples were used. The Ho^{3+} 5F_5 lifetime at 10 K was $\tau_0 \approx 1.9 \mu\text{s}$, also much smaller than the calculated radiative lifetime $\tau_r=117 \mu\text{s}$, showing again the strong Ho-host nonradiative interaction.

The decrease of the experimental lifetime with increasing temperature is usually ascribed to nonradiative release of the energy by phonon emission. These nonradiative processes are described by the characteristic nonradiative multiphonon relaxation probability $W_{\text{nr}}^{\text{ph}}=\tau_{\text{ph}}^{-1}$ and energy transfer probability $W_{\text{nr,c}}=\tau_{\text{C}}^{-1}$, which are related to the observed, τ_0^{-1} , and radiative, τ_r^{-1} , lifetimes as $\tau_0^{-1}=\tau_r^{-1}+\tau_{\text{ph}}^{-1}+\tau_{\text{C}}^{-1}$. The temperature dependence of the multiphonon relaxation rate is given by³⁸

$$W_{\text{nr}}^{\text{ph}}(T) = W_{\text{nr}}^{\text{ph}}(0) \prod_i (1 + n_{\text{eff}}^{(i)\text{ph}(i)}), \quad (1)$$

where $n_{\text{eff}}^{(i)} = [\exp(\hbar\omega_{\text{eff}}^{(i)}/kT) - 1]^{-1}$, $\hbar\omega^{(i)}$ being the energy of the i phonon emitted and k the Boltzmann constant. To main-

tain the energy conservation in a nonradiative transition between levels separated by ΔE , the gap energy must be equal to the total thermal energy released—i.e., $\Delta E = \sum_i \text{ph}^{(i)} \times \hbar\omega^{(i)}$, where $\text{ph}^{(i)}$ is the number of required i phonons. In the simplest case phonons of a single energy, usually the largest phonon observed in Raman or infrared absorption spectra, are emitted.

The analysis of the 5S_2 and 5F_5 lifetime thermal dependences with this nonradiative model produced different results. For 5S_2 the multiphonon emission model, given by Eq. (1), does not account for the behavior observed. As example, Fig. 6(b) shows (dashed line) the behavior expected for the ${}^5S_2 \rightarrow {}^5F_5$ ($\Delta E \approx 2830 \text{ cm}^{-1}$) nonradiative deexcitation by emission of three phonons with $\hbar\omega = 912 \text{ cm}^{-1}$. The assumption of a single phonon type could not reproduce neither the thermal behavior of the 5F_5 lifetime [see dashed line of Fig. 6(c)], but in this case the assumption of the emission of two phonons with $\hbar\omega = 912 \text{ cm}^{-1}$ and one of $\hbar\omega = 390 \text{ cm}^{-1}$ ($\Delta E \approx 2000 \text{ cm}^{-1}$ for the ${}^5F_5 \rightarrow {}^5I_4$ gap) provides an acceptable fit of the experimental results.

For 5S_2 it must be realized that the upper 5F_4 multiplet with lower radiative lifetime ($\tau_r = 77 \mu\text{s}$) is very close, $< 100 \text{ cm}^{-1}$ (see Table II). The increase of temperature induces a redistribution of the electronic population between 5S_2 and 5F_4 multiplets. In this case the effective radiative probability becomes temperature dependent and it can be conveniently described as³⁹

$$W_{\text{rad}}(T) = \frac{g_1 W_{\text{rad}1} \exp(-\Delta E_{1-2}/kT) + g_2 W_{\text{rad}2}}{g_1 \exp(-\Delta E_{1-2}/kT) + g_2}, \quad (2)$$

where $g_1 = 9$ and $g_2 = 5$ are the 5F_4 and 5S_2 degeneracies and $\Delta E_{1-2} \approx 100 \text{ cm}^{-1}$ is the energy gap between these two multiplets. Under this assumption the experimental 5S_2 lifetime temperature dependence can be properly described; see the solid line of Fig. 6(b).

We further studied the concentration dependence of the 5S_2 and 5F_5 room-temperature lifetimes. For the Ho concentration range available, $[\text{Ho}] < 0.6 \times 10^{20} \text{ cm}^{-3}$, all the light intensity decays observed are single exponential and the lifetime of each host remains constant. This indicates that for the Ho concentrations used nonefficient Ho-Ho energy transfer took place.

VI. DISCUSSION

First, the large linewidth of Ho^{3+} transitions in NaBiW, NaBiMo, and LiBiMo must be noted. Figure 7 shows a comparison of one of the Stark levels of the ${}^3I_8 \rightarrow {}^5F_5$ multiplet with an equivalent one corresponding to $\alpha\text{-KGdW}$, an ordered double tungstate. The FWHM of the ${}^3I_8 \rightarrow {}^5F_5$ band in NaBiW, NaBiMo, and LiBiMo is 34.5 cm^{-1} , 28.7 cm^{-1} , and 35.7 cm^{-1} , respectively. These values are about 4 times larger than the 7.7 cm^{-1} observed in $\alpha\text{-KGdW}$.

The broadening in $M^+\text{BiX}$ crystals must be understood as induced by the coexistence of several Ho environments around each of the two possible lattice sites $2b$ and $2d$. The detailed structures of these environments or the importance of their contributions to the band shape are not yet well

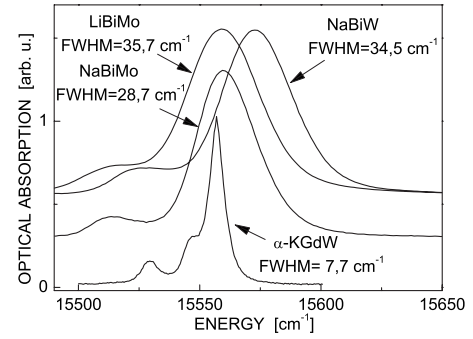


FIG. 7. Optical absorption line shape of ${}^5I_8 \rightarrow {}^5F_5$ Ho^{3+} Stark transition at 5 K in ordered monoclinic $\alpha\text{-KGdW}$ and in disordered tetragonal $M\text{Bi}(\text{XO}_4)_2$ crystals.

known but the present data show that differences between them cannot be large since, although broadened, a single band is observed at 10 K for most of the transition between Stark levels. The spectroscopic contributions of these sites have been resolved for the ${}^4F_{3/2} \leftrightarrow {}^4I_{11/2}$ Nd^{3+} transitions in NaBiW⁴⁰ and for the ${}^2F_{7/2}(0) \leftrightarrow {}^2F_{5/2}(0')$ transition of Yb^{3+} in NaGdW,¹³ NaLuW,¹⁵ and LiGdMo.²³ Similar site-resolved contributions have not been specifically searched in this work, but some of the band structures observed in Fig. 3—for instance, at $25\,824 \text{ cm}^{-1}$ (5G_4)—could be related to this fact. The polarization features shown in Figs. 1 and 3 indicate that the optical axes of all Ho centers must be close to the lattice c axis. Therefore, within the spectral resolution of our measurements the assumption of an average Ho^{3+} center to discuss the observed spectroscopic characteristics seems a good first approximation although clearly the actual situation is more complex and should include centers with symmetry lower than S_4 .

The nonradiative probability W_{nr} related to the nonradiative interaction with the host is given by the *energy gap law*

$$W_{\text{nr}} = \tau^{-1}(0 \text{ K}) - \tau_{\text{rad}}^{-1} = \beta \exp(-\alpha \Delta E_g), \quad (3)$$

where for a given lanthanide multiplet ΔE_g is the energy difference to the low-lying energy level, and α and β characterize the host. Figure 8 shows a representation of Eq. (3)

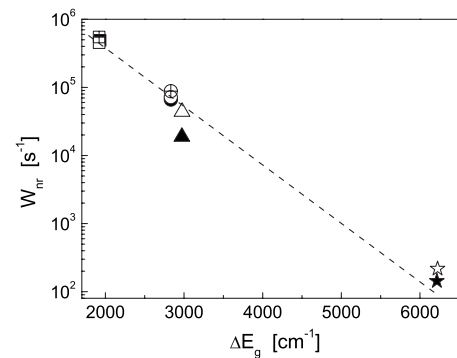


FIG. 8. Gap law representation of the nonradiative probability W_{nr} for tetragonal NaBiW (solid symbols), NaBiMo (open symbols), and LiBiMo (crossed symbols). Ho^{3+} : 5F_5 , \square ; 5S_2 , \circ . Er^{3+} : ${}^4S_{3/2}$, \triangle ; ${}^4I_{13/2}$, \star .

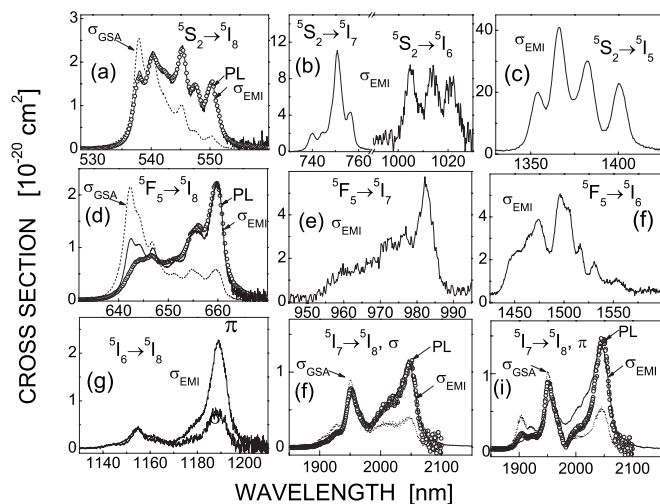


FIG. 9. Emission cross sections at 300 K of Ho^{3+} in NaBiW. The ground-state absorption cross section σ_{GSA} is indicated with the dashed line. The experimental photoluminescence by points and the calculated emission cross section σ_{emi} by the solid lines. Unpolarized ${}^5S_2 \rightarrow {}^5I_J$ (a)–(c). Unpolarized ${}^5F_5 \rightarrow {}^5I_J$ (d)–(f). Polarized ${}^5I_6 \rightarrow {}^5I_8$ (g). Polarized ${}^5I_7 \rightarrow {}^5I_8$ (f)–(i).

for the Bi-based DT and DMO. For this purpose we have used the Ho results presented in this work as well as previous results achieved for Er.¹⁶ This fit provides $\beta = 3.4 \times 10^7 \text{ s}^{-1}$ and $\alpha = 2.2 \times 10^{-3} \text{ cm}$ as average values for the three Bi-based DT and DMO hosts.

We finally discuss the emission cross sections σ_{emi} of several Ho^{3+} transitions of interest for laser application taking NaBiW for reference. σ_{emi} represents the laser gain per unit of population inversion; therefore, high values are desirable. σ_{emi} of transitions to the ground 5I_8 multiplet can be calculated from the ground-state absorption cross section $\sigma_{\text{GSA}} = \alpha_{\text{GSA}}/[\text{Ho}]$ using the reciprocity principle⁴¹

$$\sigma_{\text{emi}} = \sigma_{\text{GSA}} \frac{Z_l}{Z_u} e^{(E_{z_l} - E_{z_u})/k_B T}, \quad (4)$$

where Z_u and Z_l are the partition functions of the upper and lower multiplets, respectively, and E_{z_l} is the energy difference between the lowest Stark levels of both multiplets. For a given transition these latter parameters can be calculated from the energy-level results of Table II. For the transition to

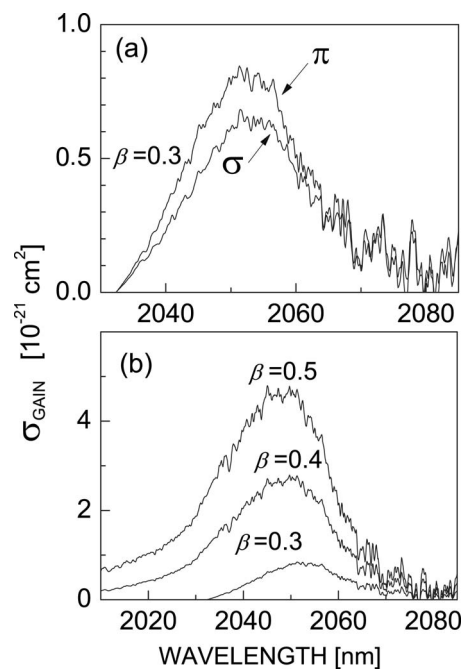


FIG. 10. Gain cross section for the ${}^5I_7 \rightarrow {}^5I_8$ transition of Ho^{3+} in NaBiW. (a) σ and π configurations. (b) Gain cross section in π configuration for increasing population inversion ratios β .

excited multiplets σ_{emi} can be obtained by the Füchtbauer-Ladensburg method:⁴²

$$\sigma_{\text{emi}} = \sigma_{\text{emi}}^{\text{ref}} \frac{I \lambda^5}{I_{\text{ref}} \lambda_{\text{ref}}^5}, \quad (5)$$

where $\sigma_{\text{emi}}^{\text{ref}}$, I_{ref} , and λ_{ref} are taken from the corresponding ${}^{2S+1}L_J \rightarrow {}^5I_8$ transition.

Figure 9 summarizes the emission cross sections of the laser channels of Ho^{3+} with the exception of ${}^5I_6 \rightarrow {}^5I_7$ ($\lambda \approx 3 \mu\text{m}$) and ${}^5I_5 \rightarrow {}^5I_6$ ($\lambda \approx 3.9 \mu\text{m}$), both expected beyond the spectral response of our equipment. Table VII shows a comparison with other laser crystal hosts taken as reference transitions to the fundamental 5I_8 multiplet. The emission cross sections obtained for Ho^{3+} in NaBiW are similar to those obtained in common oxide and fluoride laser hosts.

For transitions with the ground 5I_8 multiplet as terminal level the laser characteristics are determined by the balance between the radiative and absorption properties. This is ex-

TABLE VII. Room-temperature Ho^{3+} peak emission cross sections ($\times 10^{-20} \text{ cm}^2$) in several crystal laser hosts. In parentheses the corresponding wavelength (nm).

| | NaBi(WO ₄) ₂ | Y ₃ Al ₅ O ₁₂ ^a | YAlO ₃ ^a | YVO ₄ ^b | LiYF ₄ ^c |
|-------------------------------|-------------------------------------|---|--------------------------------|-------------------------------|--------------------------------|
| ${}^5S_2 \rightarrow {}^5I_8$ | 2.35 (545) | | | | π , 2.4 (536) |
| ${}^5F_5 \rightarrow {}^5I_8$ | 2.23 (660) | | | σ , 8.4 (660) | π , 3.3 (638) |
| ${}^5I_6 \rightarrow {}^5I_8$ | π , 2.24 (1189) | | | | π , 1.5 (1190) |
| ${}^5I_7 \rightarrow {}^5I_8$ | π , 1.45 (2047) | 1 (2090) | 1.1 (1975) | π , 2.5 (2030) | π , 2.24 (1950) |

^aReference 43.

^bReference 44.

^cReference 45.

pressed by the gain cross section σ_{gain} , defined as

$$\sigma_{\text{gain}} = \beta\sigma_{\text{emi}} - (1 - \beta)\sigma_{\text{GSA}}, \quad (6)$$

where β is the inversion ratio between fundamental and excited populations.

Figure 10 shows the $^5I_7 \rightarrow ^5I_8$ gain cross sections under different polarization and inversion ratio conditions. The wavelength corresponding to maximum σ_{gain} determines the free running laser wavelength. This occurs at 2053 nm with little difference for both polarizations. Moreover, it shifts to slightly shorter wavelength with increasing inversion ratios.

VII. CONCLUSIONS

Despite differences on the lattice cell parameters between NaBiX ($V \approx 320 \text{ \AA}^3$) and LiBiMo ($V \approx 312 \text{ \AA}^3$), the observed energy levels and radiative properties of Ho^{3+} in the three crystals remain similar each other and also close to those observed for Ho^{3+} in NaYMo ($V \approx 306 \text{ \AA}^3$). While broadened, the bands preserve well-defined S_4 polarization characteristics according to the uniaxial symmetry of the above DT and DMO crystals. These Ho^{3+} properties are representative of an average center with local S_4 symmetry for the smaller Ln^{3+} -doped structurally disordered tetragonal DT and DMO hosts with general formula $MT(\text{XO}_4)_2$. The average center

includes the effects induced by the two crystallographic sites for Ho^{3+} and the random Na^+ and Bi^+ distributions in the first cationic environment. Energy-level sequences for both NaBiW and NaBiMo have been fit very satisfactorily with rather similar sets of FI and S_4 CF parameters. The fits confirm the IR assignments derived from experiments as well as from the S_4 Er^{3+} -based initial CF simulation.

Although large nonradiative losses have been found in these DT and DMO due to large phonon energies ($\approx 980 \text{ cm}^{-1}$) associated with WO_4 or MoO_4 vibrations, the emission cross sections of Ho^{3+} in NaBiW are similar to those observed in other crystal laser hosts, and positive gain cross sections can be achieved in extended spectral ranges. These properties make the Ho^{3+} -doped double tungstates and double molybdates to be promising materials for tunable and short-pulse laser operation.

ACKNOWLEDGMENTS

This work was financed by the European Union through the DT-CRYS or NMP3-CT-2003-505580 project and by Spain through the MAT2002-04603-C05-05 (also EU FEDER found) and MAT2005-06354-C03-01 projects. A.M.B. was supported by CONACyT (México) Grant No. 128118. M.R. is supported by the Spanish Education Ministry under the ‘‘Ramón y Cajal’’ program.

*Present address Instituto de Física, Universidad Autónoma de Puebla. Apdo. Postal J-48. Puebla 72570 México.

†Corresponding author: Concepción Cascales. FAX: 34 913720623. Electronic address: ccascales@icmm.csic.es

¹E. Sorokin, I. T. Sorokina, and E. Wintner, *Appl. Phys. B: Lasers Opt.* **72**, 3 (2001).

²V. K. Tzunov, V. A. Efremov, and Y. A. Velinkodnyi, *Crystallochemistry and Properties of Double Molybdates and Tungstates* (Nauka, Leningrad, 1986) (in Russian).

³X. Huang, Z. Lin, Z. Hu, L. Zhang, J. Huang, and G. Wang, *J. Cryst. Growth* **269**, 401 (2004).

⁴V. Volkov, M. Rico, A. Méndez-Blas, and C. Zaldo, *J. Phys. Chem. Solids* **63**, 95 (2002).

⁵P. V. Klevtsov and L. P. Kozeeva, *Izv. Akad. Nauk SSSR, Neorg. Mater.* **5**, 1842 (1969) [*Inorg. Mater.* **5**, 1571 (1970)].

⁶E. Ya Rode, V. N. Karpov, and M. M. Ivanova, *Russ. J. Inorg. Chem.* **16**, 905 (1971).

⁷X. Li, Z. Lin, L. Zhang, and G. Wang, *Opt. Mater. (Amsterdam, Neth.)* **29**, 728 (2007).

⁸Yu. K. Voron'ko, K. A. Subbotin, V. E. Shukskin, D. A. Lis, S. N. Ushakov, A. V. Popov, and E. V. Zharikov, *Opt. Mater. (Amsterdam, Neth.)* **29**, 246 (2006).

⁹P. V. Klevtsov, L. P. Kozeeva, and A. A. Pavlyuk, *Sov. Phys. Crystallogr.* **20**, 736 (1976).

¹⁰P. V. Klevtsov, V. I. Maksin, R. F. Klevtsova, and A. M. Golub, *Sov. Phys. Crystallogr.* **21**, 430 (1976).

¹¹A. A. Kaminskii, S. N. Bagayev, K. Ueda, H. Nishioka, Y. Kubota, X. Chen, and A. Kholov, *Jpn. J. Appl. Phys., Part 2* **34**, L1461 (1995).

¹²A. García-Cortés, C. Cascales, A. de Andrés, C. Zaldo, E. V. Zharikov, K. A. Subbotin, S. Bjurshagen, V. Pasiskevicius, and M. Rico, *IEEE J. Quantum Electron.* **43**, 157 (2007).

¹³C. Cascales, M. D. Serrano, F. Esteban-Betegón, C. Zaldo, R. Peters, K. Petermann, G. Huber, L. Ackermann, D. Rytz, C. Dupré, M. Rico, J. Liu, U. Griebner, and V. Petrov, *Phys. Rev. B* **74**, 174114 (2006).

¹⁴J. M. Cano-Torres, M. D. Serrano, C. Zaldo, M. Rico, X. Mateos, J. Liu, U. Griebner, V. Petrov, F. J. Valle, M. Galan, and G. Viera, *J. Opt. Soc. Am. B* **23**, 2494 (2006).

¹⁵A. García-Cortés, J. M. Cano-Torres, X. Han, C. Cascales, C. Zaldo, X. Mateos, S. Rivier, U. Griebner, V. Petrov, and F. J. Valle, *J. Appl. Phys.* **101**, 063110 (2007).

¹⁶M. Rico, A. Méndez-Blas, V. Volkov, M. A. Monge, C. Cascales, C. Zaldo, A. Kling, and M. T. Fernández-Díaz, *J. Opt. Soc. Am. B* **23**, 2066 (2006).

¹⁷A. A. Kaminskii, A. Kholov, P. V. Klevtsov, and S. Kh. Khafozov, *Phys. Status Solidi A* **114**, 713 (1989).

¹⁸A. A. Kaminskii, *Crystalline Lasers: Physical processes and operating schemes* (CRC Press, Boca Raton, FL, 1996).

¹⁹A. Brenier, L. C. Courrol, C. Pedrini, C. Madej, and G. Boulon, *Phys. Rev. B* **49**, 881 (1994).

²⁰B. Yao, Y. Wang, Y. Ju, and W. He, *Opt. Express* **13**, 5157 (2005).

²¹M. A. Reis and L. C. Alves, *Nucl. Instrum. Methods Phys. Res. B* **68**, 300 (1992).

²²J. Hanuza, A. Bazar, A. Haznar, M. Maczka, A. Pietraszko, and J. H. van der Maas, *Vib. Spectrosc.* **12**, 25 (1996).

²³M. Rico, U. Griebner, V. Petrov, P. Ortega, X. Han, C. Cascales,

- and C. Zaldo, *J. Opt. Soc. Am. B* **23**, 1083 (2006).
- ²⁴A. Méndez-Blas, V. Volkov, C. Cascales, and C. Zaldo, *J. Alloys Compd.* **323-324**, 315 (2001).
- ²⁵A. Méndez-Blas, M. Rico, V. Volkov, C. Cascales, C. Zaldo, C. Coya, A. Kling, and L. C. Alves, *J. Phys.: Condens. Matter* **16**, 2139 (2004).
- ²⁶M. Rico, V. Volkov, C. Cascales, and C. Zaldo, *Chem. Phys.* **279**, 73 (2002).
- ²⁷See EPAPS Document No. E-PRBMDO-75-081717 for a brief description of the procedure followed in the crystal field analysis, its theoretical background, and the used routine IMAGE. Calculated energy levels of Ho^{3+} in $\text{NaBi}(\text{WO}_4)_2$ and in $\text{NaBi}(\text{MoO}_4)_2$, and the three main components of their associated wavefunctions are also included. For more information on EPAPS, see <http://www.aip.org/pubservs/epaps.html>.
- ²⁸C. Zaldo, M. Rico, C. Cascales, M. C. Pujol, J. Massons, M. Aguiló, F. Díaz, and P. Porcher, *J. Phys.: Condens. Matter* **12**, 853 (2000).
- ²⁹J. Kirton, *Phys. Rev.* **139**, A1930 (1965).
- ³⁰D. E. Wortman and D. Sanders, *J. Chem. Phys.* **53**, 1247 (1970).
- ³¹J. Magariño, J. Tuchendler, J. P. D'Haenens, and A. Linz, *Phys. Rev. B* **13**, 2805 (1976).
- ³²C. Görller-Walrand and K. Binnemans, in *Handbook on the Physics and Chemistry of Rare Earths*, edited by K. A. Gschneidner, Jr. and L. Eyring (Elsevier Science, Amsterdam, 1998), Vol. 25, Chap. 167, pp. 196–199.
- ³³N. C. Chang, J. B. Gruber, R. P. Leavitt, and C. A. Morrison, *J. Chem. Phys.* **76**, 3877 (1982).
- ³⁴B. R. Judd, *Phys. Rev.* **127**, 750 (1962).
- ³⁵G. S. Ofelt, *J. Chem. Phys.* **37**, 511 (1962).
- ³⁶X. Lu, Z. You, J. Li, Z. Zhu, G. Jia, B. Wu, and C. Tu, *J. Phys. D* **39**, 3755 (2006).
- ³⁷Zh. X. Cheng, Sh. J. Zhang, J. R. Han, H. Ch. Chen, Q. M. Lu, and H. C. Guo, *Cryst. Res. Technol.* **36**, 449 (2001).
- ³⁸L. A. Riseberg and H. W. Moos, *Phys. Rev.* **174**, 429 (1968).
- ³⁹K. Tanimura, M. D. Shinn, W. A. Sibley, M. G. Drexhage, and R. N. Brown, *Phys. Rev. B* **30**, 2429 (1984).
- ⁴⁰C. Cascales, A. Méndez-Blas, M. Rico, V. Volkov, and C. Zaldo, *Opt. Mater. (Amsterdam, Neth.)* **27**, 1672 (2005).
- ⁴¹D. E. McCumber, *Phys. Rev.* **136**, A954 (1964).
- ⁴²B. F. Aull and H. P. Jenssen, *IEEE J. Quantum Electron.* **18**, 925 (1982).
- ⁴³S. A. Payne, L. L. Chase, L. K. Smith, W. L. Kway, and W. F. Krupke, *IEEE J. Quantum Electron.* **28**, 2639 (1992).
- ⁴⁴R. Lisiecki, G. Dominiak-Dzik, W. Ryba-Romanowski, and T. Lukasiewicz, *J. Appl. Phys.* **96**, 6323 (2004); S. Golab, P. Solarz, G. Dominiak-Dzik, T. Lukasiewicz, M. Swirkowicz, and W. Ryba-Romanowski, *Appl. Phys. B* **74**, 237 (2002).
- ⁴⁵B. M. Walsh, N. P. Barnes, and B. Di Bartolo, *J. Appl. Phys.* **83**, 2772 (1998); B. M. Walsh, N. P. Barnes, M. Petros, J. Yu, and U. N. Singh, *J. Appl. Phys.* **95**, 3255 (2004).